1   Laser Irradiation to Produce Amorphous Pharmaceuticals

2

3   Varin Titapiwatanakun, Junlathip Tankul, Abdul W. Basit, Simon Gaisford*

4   UCL School of Pharmacy, University College London, 29-39 Brunswick Square,

5   London, WC1N 1AX, UK

6

7

8

9

10   *Corresponding author

11   email: s.gaisford@ucl.ac.uk

12   Tel: +44(0)20 7753 5863

13   Fax: +44(0)20 7753 5942

14

15

16   **Abstract**

17

18   Using a high-power CO_2 laser to irradiate powder beds, it was possible to induce

19   phase transformation to the amorphous state. Irradiation of a model drug,

20   indometacin, resulted in formation of a glass. Varying the settings of the laser (power

21   and raster speed) was shown to change the physicochemical properties of the

22   glasses produced and all irradiated glasses were found to be more stable than a

23   reference glass produced by melt-quenching. Irradiation of a powder blend of

24   paracetamol and polyvinylpyrrolidone K30 was found to produce a solid amorphous

25   dispersion. The results suggest that laser-irradiation might be a useful method for

26   making amorphous pharmaceuticals.

27

31

32

33

Introduction

The limiting factor controlling bioavailability of many actives delivered via the oral route is solubility. When an active is formulated in the stable crystalline form, solubility and dissolution rate are minimised. Poor bioavailability might be overcome by formulating the active in a metastable crystal form, although care must be taken when using this formulation strategy to ensure there is no conversion to the stable polymorph during storage. If the metastable form also does not have acceptable solubility then formulation in the amorphous state may be necessary. In cases where the drug itself is a good glass former, no excipients are necessary to stabilise the amorphous form, but for other drugs incorporation into a polymeric matrix to form a solid amorphous dispersion may be necessary.

It follows that methods that may result in phase transformation to an amorphous state will always be important, either for evaluation purposes during preformulation or for large-scale manufacture. Several methods are well known to produce amorphous materials; for instance, spray-drying, freeze-drying, melt-extrusion or melt quenching. Spray-drying requires the compound to have appreciable solubility in a suitable solvent (which is typically organic, because of the low aqueous solubility) while melt quenching requires the compound to be stable upon melting and also requires handling of cryogenic liquids, typically liquid nitrogen. Neither freeze-drying or quench-cooling are particularly suited to large-scale manufacture, although freeze-frying is used to prepare thermally-labile compounds, such as proteins, commercially. Melt-extrusion is widely use to prepare drug-polymer blends but cannot general be used to prepare amorphous samples of pure, low molecular weight compounds.

In principle, any method that can rapidly heat a material above its melt and then quench cool has the potential to cause transformation to an amorphous matrix. Since a laser is a high-energy power source, we wondered whether irradiating a sample

3

62 with a laser, in this case a carbon dioxide (CO_2) laser, might be an effective

63 approach. CO_2 lasers have many applications in the medical (tissue ablation)

64 (Landthaler et al, 2004) and chemical (fabrication of microfluidic arrays, Prakash et al,

65 2015) fields and we have recently shown that they can cause phase transformations

66 in binary powder blends to produce co-crystals (Titapiwatanakun et al, 2016). In that

67 work we posited that the laser supplied sufficient energy to the powder blend to raise

68 the temperature above the melting point and the compounds mixed and recrystallised

69 in a co-crystal lattice. However, the technique appeared to require that the

70 compounds sublimed to an appreciable extent for molecular rearrangement to occur,

71 suggesting molecular mixing occurred primarily in the vapour phase. The possibility,

72 explored in this work, is that for other compounds molecular rearrangement cannot

73 occur sufficiently rapidly, either during the heat-cool cycle or because they do not

74 vapourise, and so amorphous states may be produced. The hypothesis is tested with

75 two model systems; a pure drug substance, indomethacin, and a binary blend of drug

76 substance and excipient, paracetamol and polyvinylpyrrolidone K30. Indomethacin

77 was selected as it has low aqueous solubility and exists in the solid state in three

78 monotropically-related polymorphs (the stable γ form and the metastable α, and δ

79 forms) as well as the amorphous state and is known to be a good glass former

80 (Andronis and Zografi, 2000; Fukuoka et al, 1986; Otsuka et al, 2001; Crowley and

81 Zografi, 2002). In addition, indometacin is well-known to appear yellow in colour

82 when amorphous (Tanabe et al, 2012), providing a simple visual reference that

83 phase-conversion has occurred, and it is stable in the liquid form. Paracetamol/PVP

84 K30 was selected because PVP is known to increase the solubility of paracetamol

85 (Afrasiabi Garekani et al, 2003) and because PVP has been shown to inhibit

86 crystallization of paracetamol on storage (Miyazaki et al, 2004; Wen et al, 2008).

87

88

89

90 **Materials and methods**

91

92 Indometacin (γ form, IDM) and paracetamol (monoclinic form I, PARA) were

93 purchased from Sigma-Aldrich Ltd. Polyvinylpyrrolidone (PVP K30), was purchased

94 from Fluka Analytical (UK). All materials were used as received.

95

96 *Laser irradiation*

97 A 40W CO_2 laser (Full Spectrum Laser LLC, Las Vegas, US) was used for this study.

98 For IDM experiments, an image of a square (3cm x 3cm, 300 dpi) was used as a

99 template. IDM powder was spread in a thin layer in sample holders for the respective

100 characterisation experiments (DSC and XRPD, see below) so that no additional

101 mechanical stress needed to be applied to the sample to move it once irradiated (all

102 samples were placed with the 3cm x 3cm area so as to be irradiated by the laser).

103 The focal length of the laser was 7.4 cm. The laser allows user selection of power (P)

104 and raster speed (S); various combinations were used (P75, P50, P25, S100, S75,

105 S50; the numbers reflect the percentage of the maximum speed or power that the

106 laser could achieve). Irradiated samples were stored in a desiccator over

107 phosphorous pentoxide at ambient temperature until further analysis.

108

109 For PARA experiments, an image of a square (5cm x 5cm, 300 dpi) was used as a

110 template. Physical mixtures of PARA and PVP K30 at ratios of 30:70, 50:50 and

111 70:30 were mixed in a sample bottle. The powder blend (100 mg) was spread on

112 aluminium foil as a thin layer and placed in the working field of the laser at a focal

113 length of 6.8 cm. A range of laser scanning speeds (100 and 75%) and powers (20,

114 30, 40 and 50%) were used. Irradiated samples were transferred from the aluminium

115 foil to a small vial and stored in a desiccator over P_2O_5 until use.

116

117

5

118   *Melt quenching*

119   Crystalline IDM was melted on aluminium foil at 165 $^\circ$C for 3 min and then quench-

120   cooled by dropping into liquid nitrogen. The resulting amorphous solid was warmed

121   to room temperature before being stored in a desiccator over P_2O_5.

122

123   *X-Ray Powder Diffraction (XRPD)*

124   Data were collected on a Miniflex 600 diffractometer (Rigaku, Tokyo, Japan) with Cu

125   Kα radiation at 40 kV and 15 mA. Samples were contained within a zero background

126   holder. Scanning was performed from 5°-35° 2θ at 0.01° 2θ step size and speed 5°

127   2θ/min.

128

129   *Differential Scanning Calorimetry (DSC)*

130   DSC measurements were made with a Q2000 (TA Instruments, LLC, USA). Samples

131   (3-5 mg) were encapsulated in Tzero aluminium pans and lids. Samples were heated

132   from -50 to 175 $^\circ$C at a heating rate of 10 °C/min. Modulated Differential Scanning

133   Calorimetry (MDSC) experiments were performed using the modulated mode with an

134   underlying heating rate of 3 °C/min, a modulation amplitude of ±1 °C and a

135   modulation period of 60 s. The instrument was calibrated using a standard reference

136   material (indium, T_m = 156.6, ΔH = 28.71 J/g) in accordance with the manufacturer's

137   instructions. Data were analysed with Universal Analysis 2000 (TA Instruments, LLC,

138   USA). Experiments were performed in triplicate. Crystallization and melting values

139   are reported as extrapolated onset (T_{onset}) while glass transition temperatures (T_g),

140   are calculated as the mid-point (T_m).

141

142   *Fourier-Transform Infrared (FT-IR)*

143   Data were obtained with a 100 FT-IR spectrophotometer (Perkin Elmer). The

144   spectrum of an empty cell was used as the background. The scan was performed in

145 the range of 4000 to 650 cm^{-1} for each sample at ambient conditions. Spectrum

146 Express software (version 2008) was used to process the data.

147

148 *Scanning Electron Microscopy (SEM)*

149 Samples were mounted on an aluminium stage using adhesive tape and sputter-

150 coated with gold (Quorum model Q150, Quorum Technology, UK) at 40 mA. Images

151 were collected using an SEM (SEM, Quanta 200 FEG, FEI, Netherlands).

152

153 *Stability testing*

154 IDM samples were evaluated for stability under three conditions: at room temperature

155 over P_2O_5, at 40 ^{o}C/0% RH and 40 ^{o}C/75% RH. The physical form of the samples

156 was monitored at various time intervals with XRPD as described above.

157

158 **Results and discussion**

159 *Irradiation of indometacin*

160 Immediately following laser irradiation, a change in colour of the IDM powder from

161 white to yellow was observed and the powder bed transformed to a contiguous glass

162 (Figure 1). The yellow colour immediately indicated formation of an amorphous state

163 (Bahl and Bogner, 2008; Fukuoka et al, 1996; Heinz et al, 2007; Wu et al, 2007) and

164 occurs not because of chemical degradation but because the colour of solid organic

165 materials depends on electron delocalisation and molecular interactions (Tanabe et

166 al, 2012). Although it was not possible to measure the increase in local temperature

167 caused by irradiation, because the laser was focussed on any particular point for a

168 very short (ms) time, the fact that phase-conversion occurred indicated that the

169 temperature rise must have been greater than the melting point of indometacin (159

170 ^{o}C). It was seen that the shade of the irradiated samples differed with the level of

171 irradiation, with higher power producing darker, more translucent samples, Figure 2.

172 Reducing the focal distance to 6.8 cm caused blackening of the glass, indicative of

173 thermal degradation.

174

175 The solid state forms of the IDM samples were determined with XRPD. The

176 crystalline raw material (RM) showed a number of intensity maxima, characteristic of

177 the γ-form and consistent with literature (Aceves-Hernandez et al, 2009). The melt-

178 quenched (LN$_2$) and all irradiated samples showed broad haloes, indicating their

179 amorphous nature, Figure 3.

180

181 IDM RM showed a sharp melting endotherm at 159 ^{o}C by DSC (data not shown),

182 consistent with the γ-form. DSC data for the irradiated and melt-quenched samples

183 are shown in Figure 4. All samples exhibited a glass transition at ca. (at 38 ± 1 °C),

184 followed by crystallisation (the broad exotherms) and then melting (the sharp

185 endotherms). The glass transition values (given in Table 1) varied slightly with the

186 laser settings. Fukuoka et al (1996) showed that the T_g of indomethacin was

187 dependent on the cooling rate during formation of the glass, so it seems likely that

188 the same effect occurs here, with different laser settings causing different heating

189 and cooling rates. Similarly, the temperature at which each sample recrystallizes is

190 also seen to vary with the laser settings. This presumably also indicates that on a

191 molecular level, the degree of short-range ordering within the amorphous matrix

192 differs between the samples. This means the barrier to recrystallization is higher for

193 some samples and so the temperature at which they recrystallize increases. All

194 samples crystallise to the stable γ-form, evidenced by sharp melting around 159 ^{o}C.

195

196 FTIR spectra of the IDM samples are shown in Figure 5. The sharp bands at 1713

197 and 1690 cm^{-1} can be assigned to the asymmetric acid C=O and the benzoyl C=O

198 respectively in the crystalline γ-form (Patterson et al, 2005; Strachan et al, 2007).

199 These bands are shifted to 1708 and 1680 cm^{-1} respectively for the amorphous

200   samples, and an additional band at 1735 cm^{-1} (assigned to non-hydrogen bonded

201   C=O) is seen. The absorption bands at 1314 and 1219 cm^{-1}, within the fingerprint

202   region, were found to be broader in the amorphous samples. This suggested that

203   there was a difference between the crystalline and amorphous states in terms of

204   vibrational transitions, which indicates weaker intermolecular bonding of molecules in

205   the amorphous samples.

206

207   Samples were amorphous immediately following irradiation and showed no evidence

208   of recrystallising when stored at room temperature for 6 days (Figure 6). Upon

209   storage at elevated temperature (40 ^{o}C) but dry conditions the quench-cooled sample

210   showed the appearance of diffraction peaks after 2 days, which increased in intensity

211   after 6 days, while the S100P50 irradiated sample remained amorphous. Upon

212   storage at elevated temperature (40 ^{o}C) and humidity (75% RH) both the quench-

213   cooled sample and the S100P50 irradiated sample showed the appearance of

214   diffraction peaks after 2 days, which increased in intensity after 6 days. The S100P75

215   and S100P25 samples behaved similarly to the S100P50 sample (data not shown).

216   These observations correlate with the DSC data, in that the irradiated samples have

217   a higher barrier to recrystallization to overcome, and so are more stable on storage

218   with respect to temperature, although the presence of water acts as a plasticizer,

219   crystallising all samples.

220

221   *Irradiation of PARA/PVP K30*

222   The SEM images in Figure 7 show PARA appeared as broken needle shaped

223   crystals, whereas PVP K30 particles were irregularly rounded with cracks and

224   fissures. Irradiated blends clearly passed through a molten phase and changed in

225   visual appearance. At the lowest laser power of S100P20, separate phases of PARA

226   and PVP K30 were seen, suggesting incomplete melting of the starting materials

227   during irradiation. As the irradiation power increased to S75P40, it was evident that

228   the original morphology of the powder had disappeared and the sample appeared

229   more as a contiguous solid phase.

230

231   It was observed visually that samples irradiated at lower powers (20 and 30%) had a

232   white colour, like the physical blends, while samples irradiated at higher powers were

233   a very light yellow in colour, but showed no evidence of charring. Since PARA alone

234   when irradiated remained white it is likely that the light yellow colour came from the

235   PVP K30. It is of note that irradiation at P50 caused a very sticky thin wax to form on

236   the aluminium foil substrate, which was relatively difficult to handle. On balance,

237   irradiation at S100P30 was optimal.

238

239   The XRPD pattern of PARA shows numerous intensity maxima, consistent with

240   PARA form 1 (15.2, 17.8, 20.0, 23.1 and 24.0°), while PVP K30 exhibits a halo

241   indicating it is amorphous, Figures 8. XRPD diffraction patterns for PARA/PVP K30

242   blends are shown in Figures 8-10. It is apparent that irrespective of the drug/polymer

243   ratio, irradiating at the lowest power (S75P20) produced a material with evidence of

244   crystallinity, presumably the PARA. Using a co-solvent preparation method, de

245   Villiers et al (1998) reported similar data with crystalline PARA dispersed in PVP K30.

246   When the irradiation power increased the peaks were seen to disappear, indicating

247   complete formation of a solid amorphous dispersion, although the actual power

248   needed was dependent upon the proportion of PARA, higher drug loadings requiring

249   more power. The shape and position of the amorphous halos were different, probably

250   because of differences in orientation and conformation between PARA and K30

251   molecules via hydrogen bonding interactions, which may affect the amorphous

252   packing density of polymer chains (Murthy et al, 1993). In addition Bikiaris et al

253   (2005), reported that an increased amount of amorphous drug may contribute to a

254   change in the XRPD shape.

255

256   When analysed with DSC, those samples shown to be amorphous dispersions by

257   XRPD showed only a single glass transition (values in Table 2). Several empirical

258   equations have been derived to predict the Tg of homogeneous binary systems (for

259   instance, the Gordon-Tayor and Fox equations). The Fox equation (Fox, 1956)

260   predicts an intermediate T_g based on the weight fractions of the components;

261

262
$$\frac{1}{T_g} = \frac{W_1}{T_{g,1}} + \frac{W_2}{T_{g,2}}$$

263

264   Where W is the weight fraction of each component and the numerical subscripts refer

265   to the component materials. The glass transition temperature of pure PARA is ca.

266   25°C (Qi et al, 2008) while that of K30, measured here by DSC (data not shown), is

267   160 ^{o}C, so assuming ideal mixing, the Fox equation predicts glass transition

268   temperatures of 61.1, 43.3 and 33.5 for PARA:K30 (in ratios of 30:70, 50:50 and

269   70:30 respectively). These values correlate well with the measured temperatures of

270   42-63 °C indicating miscibility of the drug and polymer.

271

272

273   **Conclusion**

274   It has been demonstrated that irradiating crystalline powders with a high-power laser

275   causes phase transformation to the amorphous phase. Varying the laser settings of

276   power and raster speed didn't influence whether phase transformation occurred, but

277   did appear to affect the physicochemical properties of the resulting materials. Pure

278   indometacin was found to transform to a glass, which was more stable upon storage

279   than a melt-quenched reference material. Mixtures of PARA and PVP K30 were

280   found to transform to a solid amorphous dispersion at higher irradiation powers.

281   While we do not envisage laser irradiation as being a method suitable for large-scale

11

282   manufacture, it does seem to offer a new route to the amorphous form that might be

283   useful during preformulation characterisation.

284

285   **References**

286   Aceves-Hernendez, J.M., Nicolás-Vázquez, I., Aceves, F.J., Hinojosa-Torres, J., Paz,

287   M., Castaño, V.M. 2009. Indomethacin polymorphs: Experimental and conformational

288   analysis. J. Pharm. Sci., 98:2448-2463.

289   Afrasiabi Garekani, H., Sadeghi, F., Ghazi, A. 2003. Increasing the Aqueous

290   Solubility of Acetaminophen in the Presence of Polyvinylpyrrolidone and Investigation

291   of the Mechanisms Involved. Drug Dev. Ind. Pharm., 29:173-179.

292   Andronis, V., G. Zografi. 2000. Crystal nucleation and growth of indomethacin

293   polymorphs from the amorphous state. J. Non-Cryst. Solids, 271:236-248.

294   Bahl, D., Bogner, R. 2008. Amorphization alone does not account for the

295   enhancement of solubility of drug co-ground with silicate: The case of indomethacin.

296   AAPS PharmSciTech, 9:146-153.

297   Bikiaris, D., Papageorgiou, G.Z., Stergiou, A., Pavlidou, E., Karavas, E., Kanaze, F.,

298   Gerrgarakis, M. 2005. Physicochemical studies on solid dispersions of poorly water-

299   soluble drugs: Evaluation of capabilities and limitations of thermal analysis

300   techniques. Thermochim. Acta, 439:58-67.

301   Crowley, K.J., Zografi, G. 2002. Cryogenic grinding of indomethacin polymorphs and

302   solvates: Assessment of amorphous phase formation and amorphous phase physical

303   stability. J. Pharm. Sci., 91,492-507.

304   de Villiers, M.M., Wurster, D.E., Van der Watt, J.G., Ketkar, A. 1998. X-Ray powder

305   diffraction determination of the relative amount of crystalline acetaminophen in solid

306   dispersions with polyvinylpyrrolidone. Int. J. Pharm., 163:219-224.

307   Fox, T.G.B., 1956. Influence of diluent and of copolymer on the glass temperature of

308   a polymer system. Am. Phys. Soc., 1:123-125.

309   Fukuoka, E., Makita, M, Yamamura, S, 1986. Some Physicochemical Properties of

310   Glassy Indomethacin. Chem. Pharm. Bull., 34:4314-4321.

311 Heinz, A., Savolainen, M., Rades, T., Strachan, C.J. 2007. Quantifying ternary

312 mixtures of different solid-state forms of indomethacin by Raman and near-infrared

313 spectroscopy. Eur. J. Pharm. Sci., 32:182-192.

314 Landthaler, M., Ulrich, H., Hohenleutner, S., Wimmershoff, M., Hohenleutner, U.

315 2004. Role of laser therapy in dermatology – clinical aspects. Dermatology, 208:129-

316 134.

317 Miyazaki, T., Yoshioka, S., Aso, Y., Kojima, S. 2004. Ability of polyvinylpyrrolidone

318 and polyacrylic acid to inhibit the crystallization of amorphous acetaminophen. J.

319 Pharm. Sci., 93:2710-2717.

320 Murthy, N.S., Minor, H., Bednarczyk, C., Krimm, S. 1993. Structure of the amorphous

321 phase in oriented polymers. Macromol., 26:1712-1721.

322 Otsuka, M., Kato, F., Matsuda, Y. 2001. Determination of indomethacin polymorphic

323 contents by chemometric near-infrared spectroscopy and conventional powder X-ray

324 diffractometry. Analyst, 126:1578-1582.

325 Patterson, J.E., James, M.B., Forster, A.H., Lancaster, R.W., Butler, J.M., Rades, T.

326 2005. The influence of thermal and mechanical preparative techniques on the

327 amorphous state of four poorly soluble compounds. J. Pharm. Sci., 94:1998-2012.

328 Prakash, S., Kumar, S. 2015. Fabrication of microchannels on transparent PMMA

329 using CO2 laser (10.6 μm) for microfluidic applications: An experimental

330 investigation. Int J Pres Eng Manufac., 16:361-366.

331 Qi, S., Avalle, P., Saklatvala, R., Craig, D.Q.M. 2008. An investigation into the effects

332 of thermal history on the crystallisation behaviour of amorphous paracetamol. Eur. J.

333 Pharm. Biopharm., 69:364-371.

334 Strachan, C.J., Rades, T., Gordon, K.C. 2007. A theoretical and spectroscopic study

335 of γ-crystalline and amorphous indometacin. J. Pharm. Pharmacol., 59:261-269.

336 Tanabe, S., Higashi, K., Umino, M., Limwikrant, W., Yamamoto, K., Moribe, K. 2012.

337 Yellow coloration phenomena of incorporated indometacin into folded sheet

338 mesoporous materials. Int. J. Pharm., 429:38-45.

339   Taylor, L., Zografi, G. 1997. Spectroscopic Characterization of Interactions Between

340   PVP and Indomethacin in Amorphous Molecular Dispersions. Pharm. Res., 14:1691-

341   1698.

342   Titapiwatanakun, V., Basit, A.W., Gaisford, S. 2016. A new method for producing

343   pharmaceutical co-crystals: Laser irradiation of powder blends. Cryst. Growth Des.

344   DOI:10.1021/acs.cgd.6b00289.

345   Wen, H., Morris, K., Park, K. 2008. Synergic Effects of Polymeric Additives on

346   Dissolution and Crystallization of Acetaminophen. Pharm. Res., 25:349-358.

347   Wu, T., Ye, S., Li, N., de Villiers, M.M., Yu, L. 2007. Inhibiting Surface Crystallization

348   of Amorphous Indomethacin by Nanocoating. Langmuir, 23:5148-5153.

349

350

351

352

353

Sample	T_g (^{o}C)	$T_{recryst}$ (^{o}C)	T_m (^{o}C)
LN2	39.2	84.9	158.7
S100P25	36.9	88.6	159.8
S100P50	38.1	101.7	158.7
S100P75	39.1	107.0	157.9

354

355 **Table 1: Phase transition temperatures for melt-quenched and laser-irradiated**

356 **IDM samples from DSC data**

357

358

Sample	Irradiation setting	T_g ($_o$C)
30:70 PARA:PVP K30	S100P50	47.0
30:70 PARA:PVP K30	S40P75	51.2
30:70 PARA:PVP K30	S50P75	63.6
50:50 PARA:PVP K30	S50P75	41.9

359

360 **Table 2. Glass transition temperatures determined by MDSC for various solid**

361 **amorphous dispersions**

362
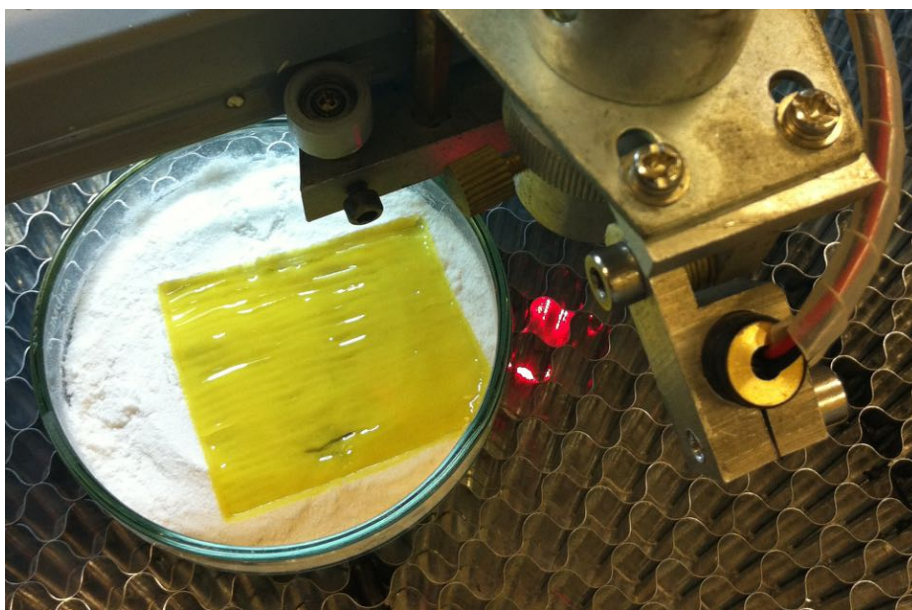
363

364

365   **Figure 1. IDM sample during irradiation with the CO_2 laser, showing crystalline**

366   **powder around the edge and a glass in the 3 x 3 cm square exposed to the**

367   **laser beam**

368

369

370

371

Figure 2: Images of laser-irradiated IDM samples at various speed (S) and power (P) settings. From top to bottom, S100P25, S75P25, S50P25 all at a focal length of 7.4 cm and S100P25 at a focal length of 6.8 cm.

375

376

377
378

379

380

Working distance at 7.4 cm
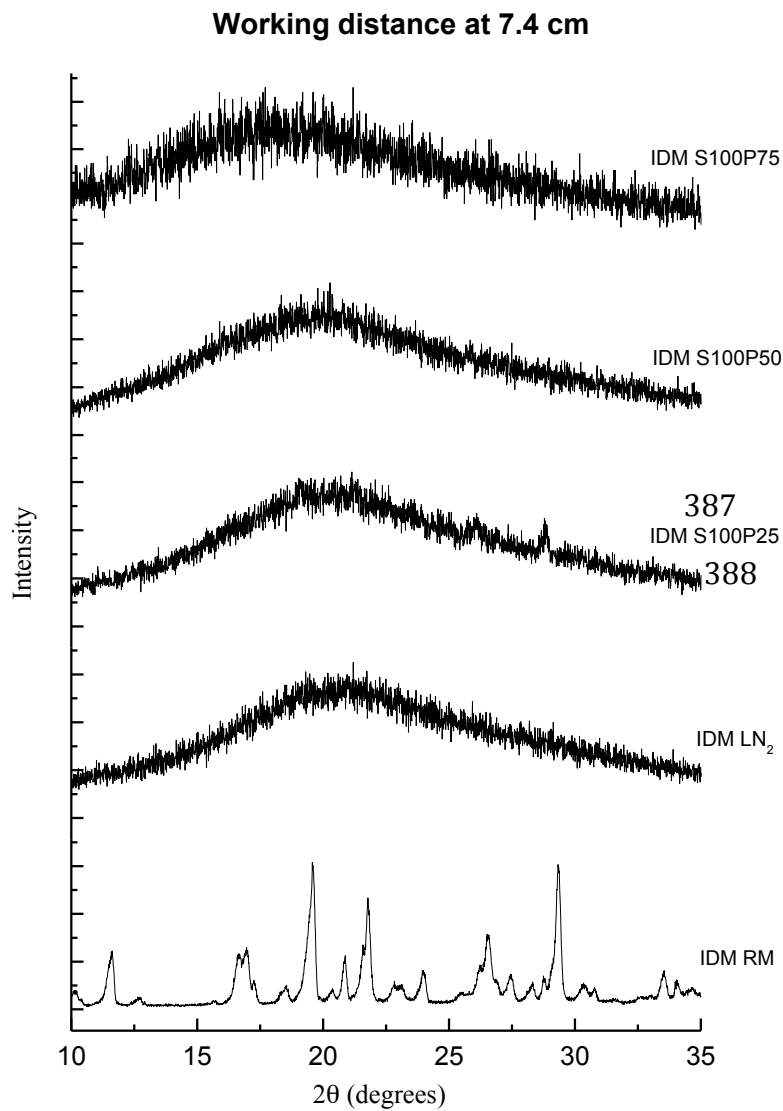
Figure 3. XRPD diffraction patterns for IND raw material (RM), melt quenched (LN$_2$) and laser-irradiated at various settings of speed (S) and power (P).

405
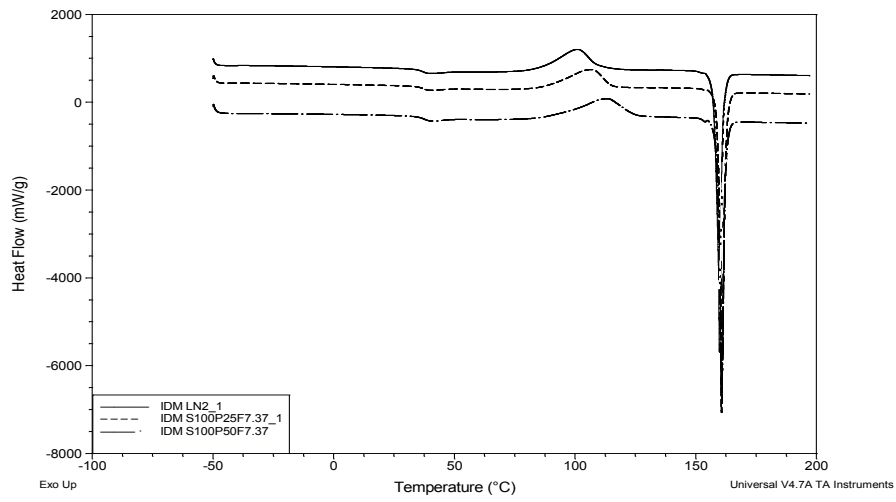
406

407

408

409 **Figure 4. DSC traces for the melt-quenched (LN2) and laser-irradiated**

410 **(S100P25, S100P50 and S100P75) IDM samples.**

411

412
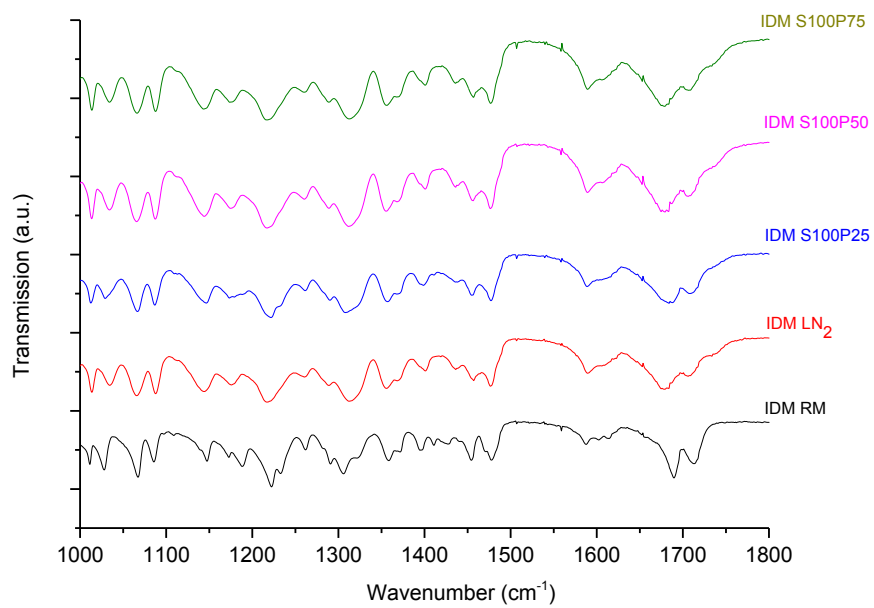
Figure 5. FTIR spectra for the raw material (RM), melt-quenched (LN2) and laser-irradiated (S100P25, S100P50 and S100P75) IDM samples.

413

414

415

416

417

418

419

420

421
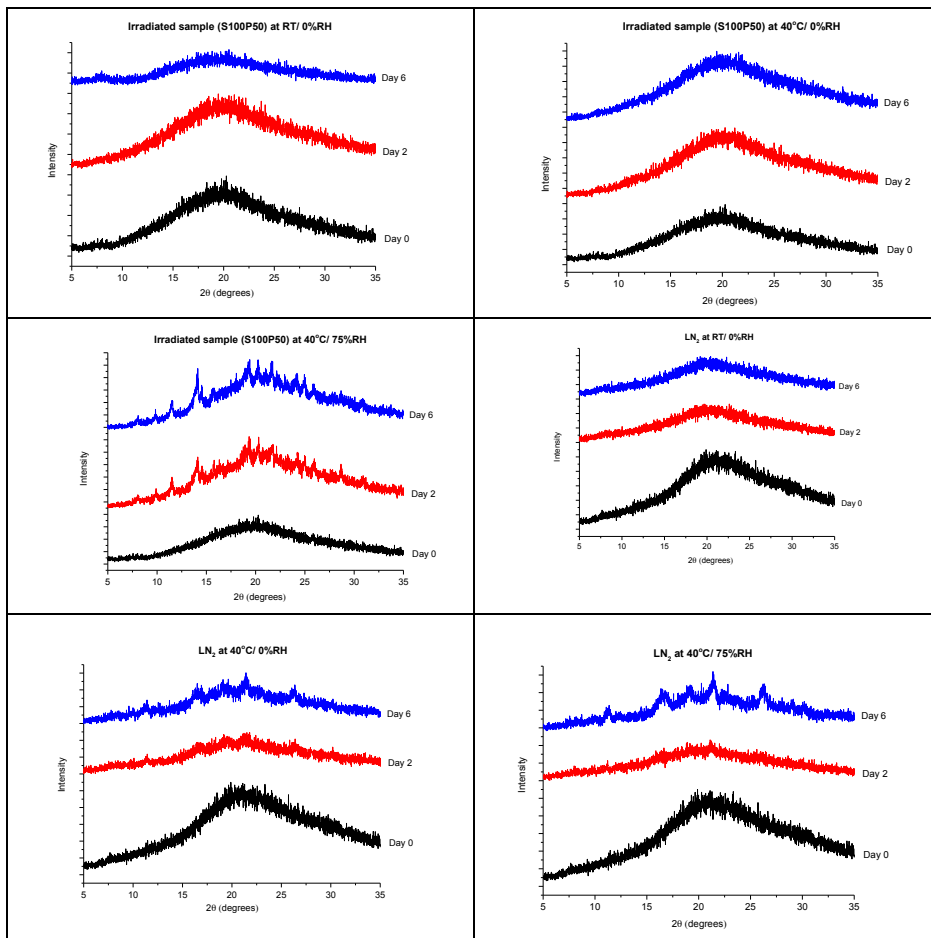
Figure 6. XRPD diffraction patterns for quench-cooled (LN2) and laser-irradiated (S100P50) IDM samples as a function of time and storage conditions.

422

423

424

425
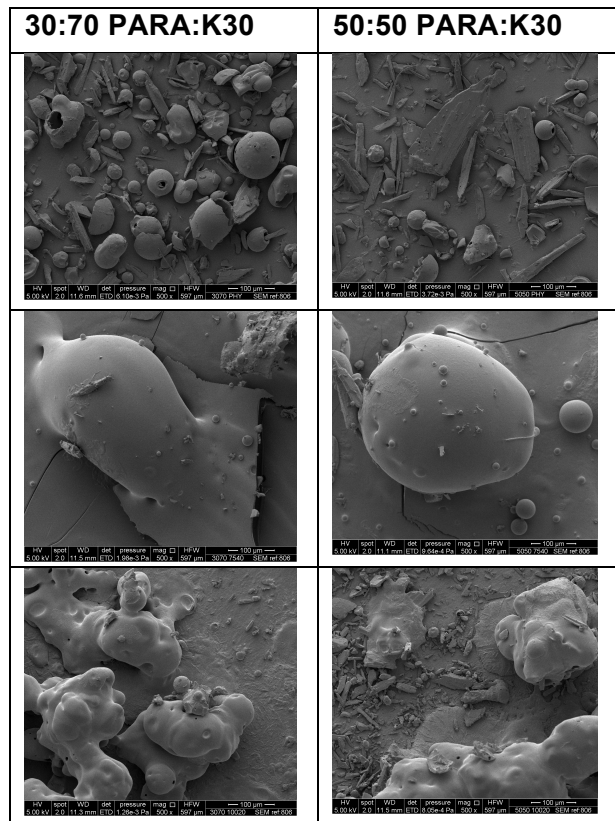
Figure 7: SEM images of PARA:PVP K30 physical mixture (top) and 30:70 and 50:50 mixtures following irradiation at S75P40 (middle) and S100P20 (bottom).

432
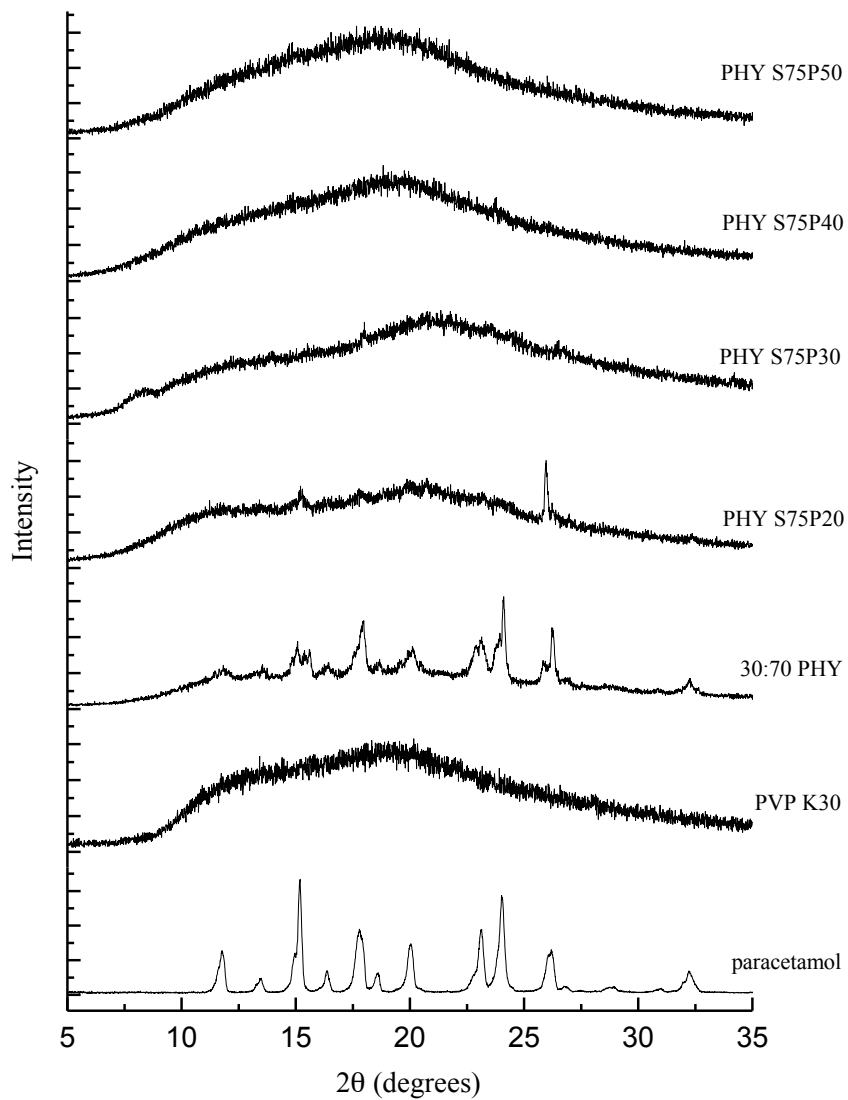
Figure 8. XRPD diffraction patterns for PARA raw material, PVP K30 raw
material and 30:70 PARA:PVP K30 mixtures irradiated with different laser
powers

433

434

435

436

437
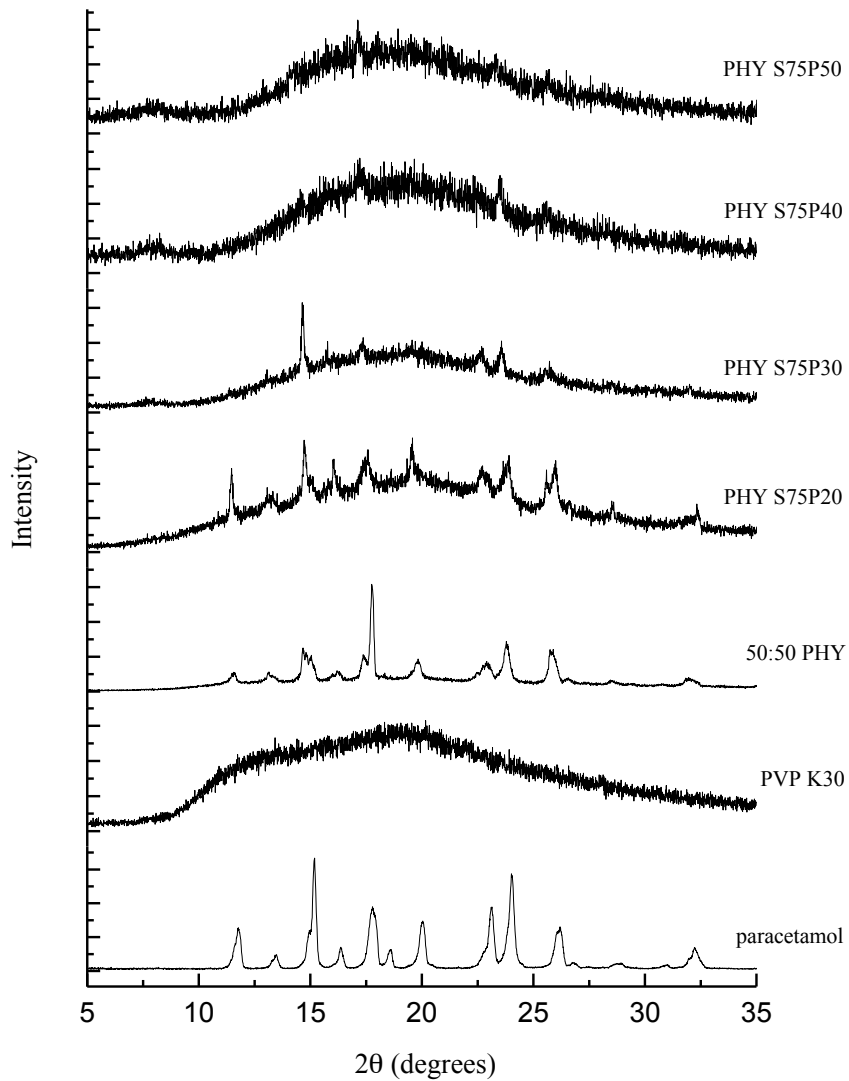
Figure 9. XRPD diffraction patterns for PARA raw material, PVP K30 raw material and 50:50 PARA:PVP K30 mixtures irradiated with different laser powers
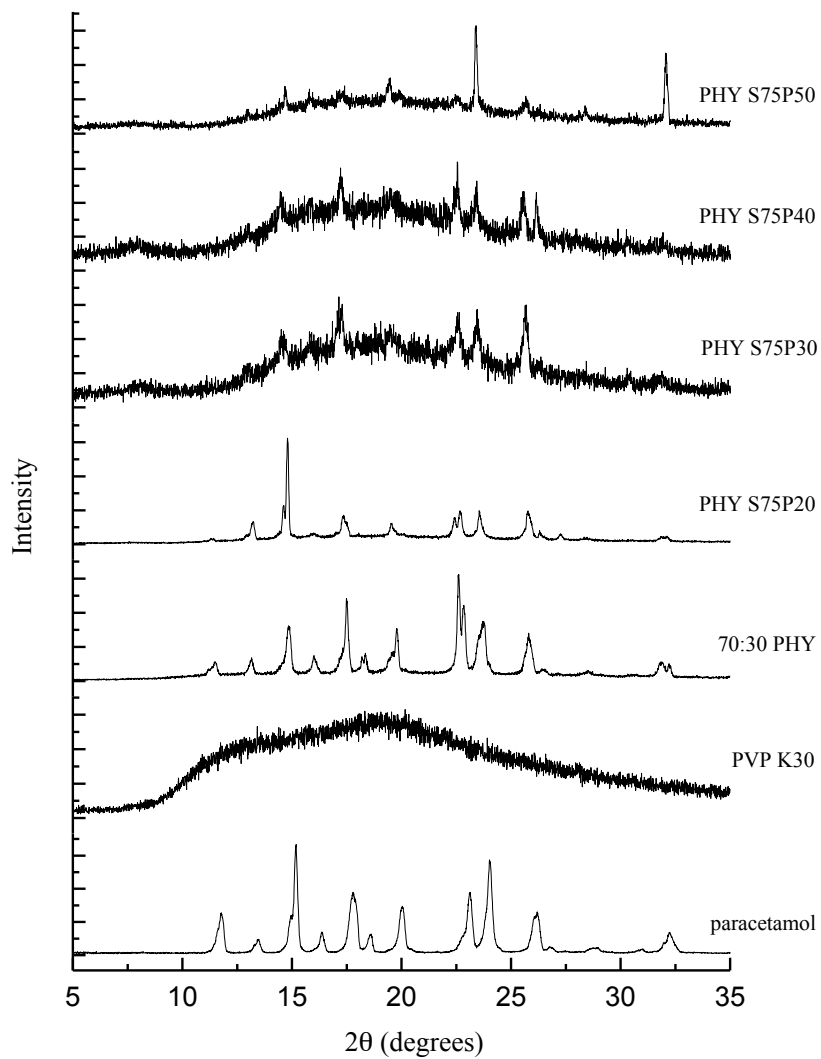
Figure 10. XRPD diffraction patterns for PARA raw material, PVP K30 raw material and 70:30 PARA:PVP K30 mixtures irradiated with different laser powers